In Vivo Multiple-Mouse MRI at 7 Tesla

Nicholas A. Bock,*[1,2] Brian J. Nieman,[1,2] Johnathan B. Bishop,[1] and R. Mark Henkelman[1,2]

We developed a live high-field multiple-mouse magnetic resonance imaging method to increase the throughput of imaging studies involving large numbers of mice. Phantom experiments were performed in 7 shielded radiofrequency (RF) coils for concurrent imaging on a 7 Tesla MRI scanner outfitted with multiple transmit and receive channels to confirm uniform signal-to-noise ratio and minimal ghost artifacts across images from the different RF coils. Grid phantoms were used to measure image distortion in different positions in the coils. The brains of 7 live mice were imaged in 3D in the RF coil array, and a second array of 16 RF coils was used to 3D image the whole bodies of 16 fixed, contrast agent-perfused mice. The images of the 7 live mouse brains at 156 μm isotropic resolution and the 16 whole fixed mice at 100 μm isotropic resolution were of high quality and free of artifacts. We have thus shown that multiple-mouse MRI increases throughput for live and fixed mouse experiments by a factor equaling the number of RF coils in the scanner. Magn Reson Med 54:1311–1316, 2005. © 2005 Wiley-Liss, Inc.

Key words: parallel imaging; mouse imaging; phenotyping; mouse models of disease; high field

Magnetic resonance imaging (MRI) now has a strong role to play in the characterization of genetically altered mice from transgenic and knockout studies, random mutagenesis programs, and the search for mouse models of human disease. It is also used to study traditional mouse models of disease, such as mice bearing tumor xenografts and stroke. It is useful for mouse imaging because it is an in vivo modality that provides good soft tissue contrast (1–4). Since the morphologic phenotype of a mouse may be unknown, whole-body 3D imaging at a high resolution is needed to detect abnormalities and quantify their size and shape accurately without partial-volume effects. Also, if one assumes about a 1:15 linear dimension scaling factor between structures in mice and humans, then the resolution in mouse MRI should be about 15 times finer than that of human imaging to produce comparable definition in the image. By using specialized radiofrequency (RF) coils and high magnetic field strengths, this resolution can be approached in live mice, although the loss of sensitivity from the diminishing voxel size means imaging times need to be on the order of hours to produce useful signal-to-noise ratios (SNRs). As well, typical biologic experiments require dozens of mice to produce statistically significant data. Hence, small animal MRIs that can scan only 2 or 3 mice a day are inadequate. To overcome the inherently low throughput in MRI, several techniques have been shown to image multiple mice at once in the same MRI scanner (5–9). Here we present a high-field, live multiple-mouse MRI technique (MMMRI) that increases the number of mice imaged considerably without increasing the imaging time nor sacrificing SNR.

METHODS

In our MMMRI method, described in detail in (9), we use a separate, shielded transmit/receive RF coil for each mouse with its own receiver in a large bore magnet and a shared (6) or distributed gradient set. Up to 16 cylindrically shielded RF coils are closely packed in a hexagonal array (dubbed the Mousehive) within a common gradient set and magnet (Fig. 1). To reduce the size of the images and to preserve the imaging time for one mouse, the field of view (FOV) is set to cover just one mouse, and the other mice are spatially encoded by replicated FOVs. For a 3D image, the readout gradient is set along the long axis of a mouse and is common to all mice, so they will be spatially encoded identically in that direction. The phase-encoding gradients are applied in the x and y directions over one mouse, and their FOVs are tiled across the bore of the gradient through the periodicity property of the discrete Fourier transform. Since the spacing of the replicated FOVs does not coincide with the positions of all the mice, some appear aliased in the resulting images (Fig. 1) but can be centered by multiplying the raw *k*-space data by a factor of $\exp(-i2\pi(k_x x + k_y y))$, where x and y are the displacements of the mouse with respect to the isocenter of the gradients. More easily, the images can be cut and pasted back together to correct the wrapping—a step that we have automated.

Limiting the FOV to a single mouse while acquiring data from multiple mice can also be applied to non-Cartesian imaging, such as radial and spiral, although the off-centered FOVs do not produce the simple wrapping artifact seen in Cartesian imaging. However, the artifacts in mice whose positions are off the isocenter of the gradients can again be corrected by multiplying the raw *k*-space data by a phase correction factor that depends on both the mouse's position in the bore of the gradient and the gradient waveforms that are used for spatial encoding.

Ideally, since the RF coils are electrically shielded and have their own receivers, neither the signal nor the noise in any one coil is affected by the addition of other coils. If, however, there is reactive coupling between RF coils, cables, or receiver channels on the scanner, the coupling can be corrected (10) for by using a SENSE-like method that can remove the overlapping image ghosts with no noise penalty (11).

To validate multiple-mouse MRI, we performed a series of experiments on a 7 Tesla 40 cm bore magnet (Magnex

[1]Department of Medical Biophysics, University of Toronto, Toronto, Canada.
[2]Mouse Imaging Centre (MICe), Hospital for Sick Children, Toronto, Canada.
*Correspondence to: Nicholas Bock, Mouse Imaging Centre, Hospital for Sick Children, 555 University Avenue, Toronto, Ontario, Canada, M5G 1X8. E-mail: nbock@sten.sunnybrook.utoronto.ca

Received 31 March 2005; revised 5 July 2005; accepted 8 July 2005.
DOI 10.1002/mrm.20683
Published online 7 October 2005 in Wiley InterScience (www.interscience.wiley.com).

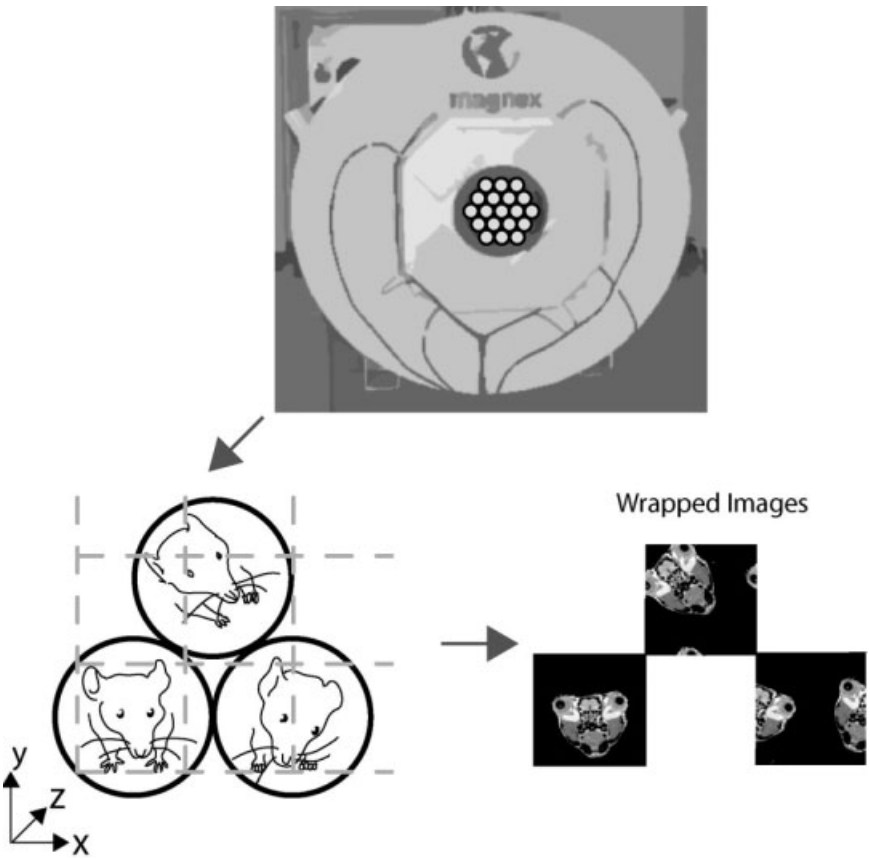

FIG. 1. (**Top**) The magnet is loaded with a hexagonal array of cylindrical volume RF coils (16 plus 3 spares) for mouse imaging. (**Left**) A field of view (FOV) is set over one mouse in the array for 3D imaging with the readout axis along the mice in the z-direction. (**Right**) Mice that are not centered in an FOV appear aliased in the reconstructed images.

Scientific, Oxford, UK) with a Varian INOVA console (Varian NMR Instruments, Palo Alto, CA) and a 29 cm inner bore gradient set (Tesla Engineering Ltd., Sussex, UK) with 120 mT/m maximum amplitude and 870 μ s rise time. The system had a custom designed set of multiplexers to switch 4 transmitters and 4 receivers among up to 16 individual RF coils. We imaged with an array of 7 many-rung birdcage coils of Varian's Millipede design (12), each with a 3.0 cm inner diameter and a length of 7.0 cm concentrically mounted in a 5.0 cm diameter cylindrical copper foil shield 40 μm thick and 19.0 cm long. The RF coils were designed to minimize reactive coupling between coils or inductive coupling between coils and the mice in other coils. The coils had a 3.5 cm long B_1 FOV with 90% homogeneity, which was useful for imaging specific organs in mice, like the brain.

We performed phantom-based experiments to test the SNR in the RF coil array and the electrical coupling between coils and channels on the scanner. Each of the 7 coils was loaded with a 10 mL cylindrical 2% agar sample designed to electrically load the coils similarly to a mouse's head. A 2D image with an FOV covering the entire 7 coil array (spin-echo, frequency x phase = 512 $\times$ 256, FOV = 20 $\times$ 20 cm, slice = 1 mm, TR/TE = 300/18 ms, NEX = 60) was collected to obtain a large SNR. This allowed the measurement of weak image ghost interactions caused by coil coupling above the noise floor of each image. Since we only have 4 parallel receivers on our scanner, we used multiplexing for imaging. For each acquisition, we switched the transmitters and receivers to one group of 4 coils and performed an excitation and reception in parallel, then switched to the second group of 3 coils to collect the same acquisition step in the other coils during the 300 ms repetition time (TR) for the first group. Because we were able to perform the multiplexing within the TR for the first group, our imaging time was not increased. Our gradient achieves a minimum TR of 50 ms, which is quadrupled with the multiplexing. We imaged with a large FOV that covered the entire RF coil array so any ghosts would not be overlapping in the images. We measured the coupling by quantifying the ghosts in the magnitude images from each channel. This measurement accounted for all the coupling between channels on the system from the RF coils to the receivers.

To ensure a good B_0 and gradient field over the volume needed for whole-body imaging in an array of 16 mice, the B_0 field of the magnet was shimmed during installation to 20 ppm over a 27 cm diameter $\times$ 14 cm long cylinder at the isocenter of the magnet. The linear region of the gradients was defined over a 25 $\times$ 11 cm oblate spheroid within that region. Since the dimensions of the mice are small compared to the dimensions of the gradient and magnet coils, the actual field inhomogeneities should be small over each mouse, even if they are large over the entire volume of the RF coil array. Further shimming using electrical shim coils, however, is only possible on the volume of mice as a whole, because shimming in one mouse will interact with and deteriorate the shim in other mice. This means that B_0 inhomogeneities may persist, introducing minor distortions in images and limiting the usefulness of

Table 1
Isolation Between Images in dB on a 7 RF Coil MMMRI System. Coil Groups 1–4 and 5–7 Were Multiplexed.

Images	1	2	3	4	5	6	7
1	0	−58	−54	−56	−56	−54	−55
2	−58	0	−51	−58	−51	−58	−54
3	−59	−61	0	−61	−61	−58	−59
4	−58	−50	−58	0	−55	−56	−56
5	−59	−58	−58	−58	0	−58	−47
6	−58	−58	−56	−58	−58	0	−58
7	−63	−63	−62	−63	−54	−61	0

MMMRI for applications that need a very good shim, like spectroscopy. To measure image distortion (which could confound phenotyping efforts) over the regions covering the mouse brains, we used 2 grid phantoms. One phantom consisted of a 15 × 15 mm array of 25, 0.5 mm holes drilled in acrylic in the xy plane with a spacing of 3 mm, while a second phantom consisted of the same array drilled in the xz plane. Both phantoms were filled with water doped with 0.5 mM $CuSO_4$ and 1.4 mM NaCl. We used an average shim for the array of coils and imaged the phantoms in each coil with a multi-slice sequence of 20 contiguous 1 mm thick slices (spin-echo, frequency x phase = 128 × 128, FOV = 20 × 20 mm, slice = 1 mm, TR/TE = 3000/20 ms, NEX = 1). The unused coils in the array were loaded with phantoms to simulate mouse heads. We found the centroids of the grid point images in each slice using Matlab (v 6.5.0 release 13, The MathWorks Inc, Natick, MA) to compare the resulting grid spacing to the actual grid spacing in the phantom.

Following these phantom experiments to assure the performance of multiple-mouse MRI, we imaged live female C3H mice (The Jackson Laboratory, Bar Harbor, ME), which weighed about 25 grams each. All animal experiments were approved by the Animal Care Committee at the Hospital for Sick Children. The mice were injected intraperitoneally (i.p.) (13) 48 h prior to imaging with 20 mM/kg $MnCl_2$, which is taken up through voltage-gated Ca^{2+} channels in neurons and acts as a positive contrast agent when it accumulates in brain structures (14). Live multiple-mouse imaging requires streamlined mouse handling to maintain its high throughput and to maximize the time available for imaging. Each mouse must also be monitored over the course of imaging to assess its level of anesthetization and body temperature. While necessary changes to anesthetic and heating might be made on a per mouse basis, we found that mice of the same weight and lineage could all be supported using the same levels of anesthetic and heating. We prepared the mice in an induction chamber filled with 4% isofluorane anesthetic gas in 100% O_2 by shaving their chests so that they could lie on specialized sleds (15) in contact with ECG leads and a thermocouple skin temperature probe that allows us to monitor their temperature and adjust it manually during imaging with blown warm air. The mice on the sleds were placed in centrifuge tubes and mounted onto a loading array. This array docked with the hexagonal array of coils resident in the bore of the magnet, and our total preparation time for the 7 mice was under half an hour. The mice were anesthetized during imaging with 1–2% isofluorane gas in 100% O_2 delivered via nose cones. We imaged the heads of the mice with a 3D T_1-weighted sequence (spin echo, frequency × phase × phase, FOV = 256 × 128 × 128, FOV = 40 × 20 × 20 mm, TR/TE = 300/8 ms, NEX = 2) to produce 156 μm isotropic voxels in 2 h and 45 min. The images were reconstructed in parallel on an SGI Origin 2000 with 32 CPUs and 32 gigabytes of RAM (Silicon Graphics, Mountain View, CA).

We are currently limited to imaging 7 live mice because of a lack of physiologic monitoring channels; however, we ultimately wish to image the whole bodies of 16 live mice at once. Therefore, we also used a second RF coil array of 16, 11 cm long Millipede coils to image 16 formalin-fixed C3H mice (The Jackson Laboratory, Bar Harbor, ME) of 20–30 grams (live) weight perfused with 10 mM gadopentetate dimeglumine (Magnevist, Berlex Canada Inc., Canada). The mice were perfused through the left ventricle under ultrasound guidance, which preserved the integrity of the chest and the abdominal cavity. We imaged the mice with a 3D T_1-weighted pulse sequence (spin echo, frequency × phase × phase = 960 × 270 × 270 = 96 × 27 × 27 mm, TR/TE = 650/15ms, NEX = 1) that produced 100 μm isotropic voxels in about 13 h.

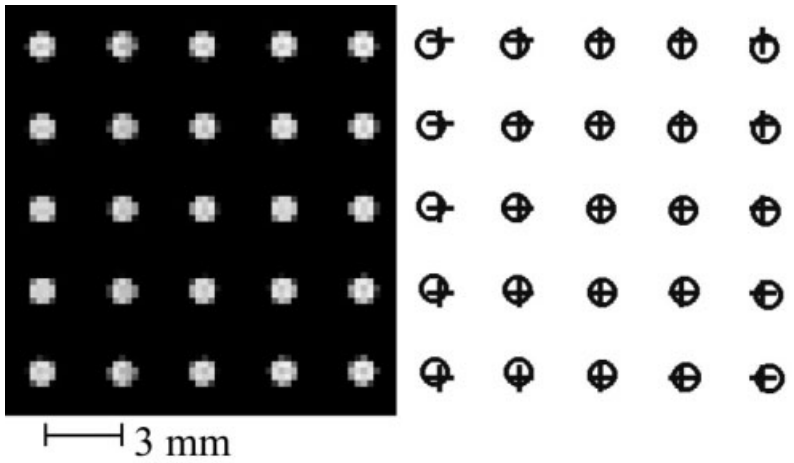

FIG. 2. (**Left**) One slice from an MR image of a grid phantom imaged in the xy plane. (**Right**) The centroid of each grid point is found (circles) and plotted against the actual grid spacing of the phantom (crosses) to illustrate distortion.

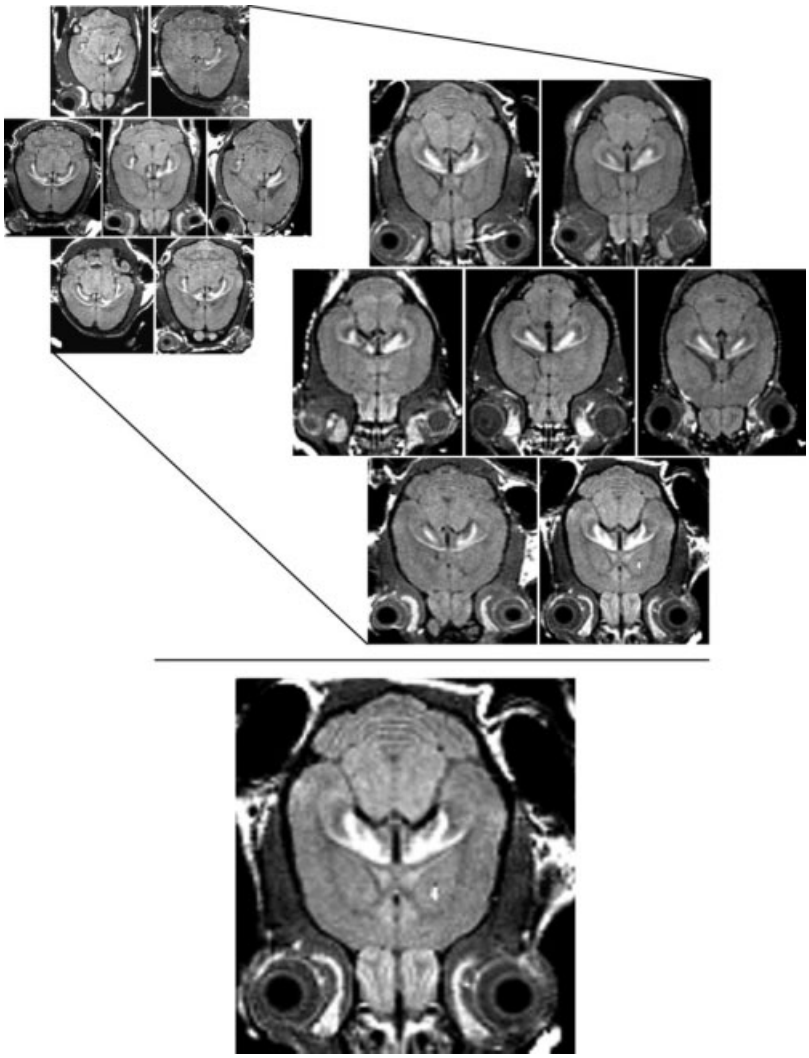

FIG. 3. (**Upper Left Inset**) One slice each from seven 156 μm isotropic 3D brain images of mice imaged with MMMRI. Regions of high neuronal density or activity appear bright in the T_1-weighted images because Mn^{2+} has accumulated there. (**Middle**) The 3D images were registered into a common stereotaxic space and redisplayed at the same horizontal plane in each mouse. (**Bottom**) An enlarged view of one of the mouse brain images.

RESULTS

The mean SNR (±SD over the 7 coils) in the multiple-coil phantom magnitude images was 1500 ± 200, which was comparable to an SNR of 1400 in an image acquired in a single coil and phantom with the same imaging parameters.

From this same data set, we measured a region-of-interest (ROI) in each image j at the actual location of the phantom (ROI_j) and also an ROI at each ghost location in the other images i (ROI_i). We calculated the isolation (in dB) as:

$$\text{Isolation}_{i,j} = 20 \log_{10}\left|\frac{ROI_i}{ROI_j}\right| \qquad [1]$$

where we divided each different ROI_i by ROI_j. Table 1 shows the 7 × 7 isolation matrix we calculated between pairings of the 7 coils—the worst case isolation is −47 dB, which corresponds to a magnitude ghost image of only 0.43%. Thus, the MMMRI technique preserves SNR and imaging time from a single-mouse imaging experiment, and it is not necessary to correct for ghosts using SENSE because of the excellent isolation between images.

An image of a slice from the grid phantom used to measure distortions is shown in Fig. 2. The centroid of each image point was calculated using Matlab and was compared with the actual location of the drilled hole in the phantom. We found the average percentage distortion in each RF coil position from the images of the grid phantoms by the formula:

$$\text{Distortion} = \frac{\langle \text{Distance} \rangle}{\text{FOV}} \times 100\% \qquad [2]$$

where <Distance> was the mean distance between all the image grid points and their corresponding phantom drilled holes. FOV was the linear dimension across the phantom (1.5 cm). The average distortion (±SD across 7 coils) was 3.0 ± 0.9% in the xy plane and 3.3% ± 1.1% in the xz plane, which is similar to the distortion expected on a human clinical scanner over a typical head FOV dimension.

The 7 live images of the mice are shown in the upper left of Fig. 3, with horizontal slices at the same level of the hippocampus. The slightly different positions of the mice during scanning make it difficult to compare anatomy

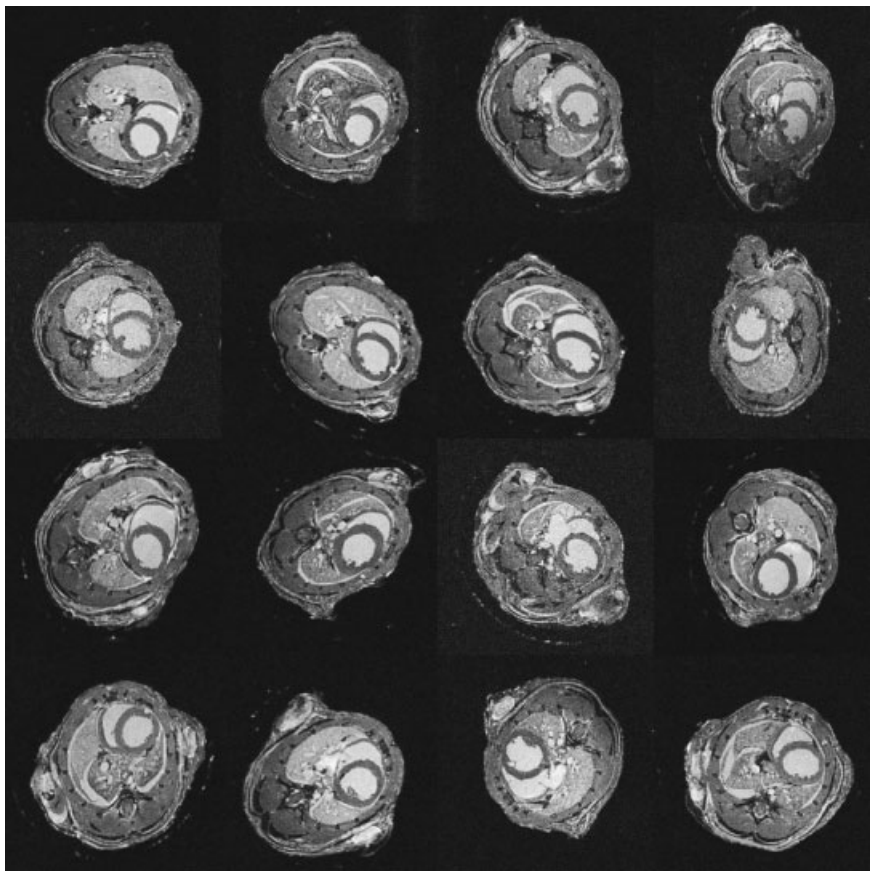

FIG. 4. One axial slice in the thorax of each mouse at the level of the cardiac ventricles from an MMMRI of 16 contrast-perfused fixed mice.

between the mice, so we performed a linear affine registration using Register software (Montreal Neurologic Institute, Montreal, Canada) to place the mice in the same stereotaxic space. The registration was based on anatomic landmarks in each mouse's head. The 7 images from each of the registered mice are shown in the center of Fig. 3 at the same horizontal level, and an enlarged image of 1 slice is provided to show image detail. Fig. 4 shows 1 axial slice from each of the 16 fixed mice at the level of the heart. The SNR and contrast differ slightly between the images due to variations in the perfusion of the contrast agent and the loading of the RF coils by the differently sized mice.

DISCUSSION

All 7 of the live brain images from the MMMRI are of a similar high quality and are suitable for phenotyping major structures in the mouse brain. They are also equivalent in quality to a slice from an image of a single mouse with the same imaging parameters. It is important to collect high resolution 3D images with isotropic resolution for phenotyping since 2D imaging can misrepresent small structures because of misalignment of slices and partial-volume artifacts—this can be seen by comparing the 2 data sets of the same brains in different orientations in Fig. 3. The images of the fixed mice are of comparable quality, which demonstrates that MMMRI can be used for very high throughput studies although the motion artifacts from breathing and cardiac motion will need to be overcome for whole-body phenotyping.

In MMMRI, there are limitations (mostly in hardware) that currently keep it from achieving its ultimate throughput in all applications. Since the mice share a common, large-bore gradient that has a lower strength and slew rate than a dedicated small animal gradient, some high speed imaging sequences are not possible. One method to overcome this would be to image each mouse in its own gradient or in a distributed winding of a single gradient (6), although this would increase the complexity of the equipment setup. The 4-way multiplexing on our current system also quadruples our gradient duty cycle, which further curtails high speed imaging applications. Currently, however, we are interested in 3D anatomic screening and do not find the gradient strength or the duty cycle on our system particularly limiting. For the future, we are developing 19 independent receivers for high speed imaging applications, such as FSE (16), that require shorter TRs and greater data acquisition duty cycles. Finally, the mice themselves present a limitation because their breathing rates and heart rates are not in synchrony, ruling out the usual prospective motion gating methods for mice (17). Retrospective gating is commonly used in human cine imaging (18), and this procedure will be used to correct for motion in multiple mouse imaging. We will need to implement such a motion correction method for imaging the whole body, the heart, and other organs that move with respiration. Despite these limitations, MMMRI already is a viable technique for improving the throughput in MRI experiments, and will become even more useful with

higher performance gradients, individual receivers for each mouse, and new motion correction procedures.

CONCLUSIONS

We have shown that MMMRI improves the throughput in mouse MRI experiments by the number of RF coils that can be placed in the bore of the gradient and will make future studies scientifically significant by increasing the number of animals. Considerable effort has been put into developing clinical MRI systems with multiple transmitters and receivers, and these developments benefit our technique. In the future, one could incorporate phased-array coils (19) into multiple-mouse MRI. While we have only shown MMMRI in mouse brains to limit motion effects, whole-body screening will be possible when a retrospective gating method to decrease motion artifacts and more efficient pulse sequences to increase image averaging are available. This will allow the full power of MRI to be used for mouse phenotyping and disease screening studies.

REFERENCES

1. Wiesmann F, Szimtenings M, Frydrychowicz A, Illinger R, Hunecke A, Rommel E, Neubauer S, Haase A. High-resolution MRI with cardiac and respiratory gating allows for accurate in vivo athleroschlerotic plaque visualization in the murine aortic arch. Magn Reson Med 2003;50:69–74.
2. Zhang J, Richards LJ, Yarowsky P, Huang H, van Zijl PC, Mori S. Three-dimensional anatomical characterization of the developing mouse brain by diffusion tensor microimaging. Neuroimage 2003;20:1639–1648.
3. Pautler RG, Koretsky AP. Tracing odor-induced activation in the olfactory bulbs of mice using manganese-enhanced magnetic resonance imaging. Neuroimage 2002;16:441–448.
4. Moats RA, Velan-Mullan S, Jacobs R, Gonzalez-Gomez I, Dubowitz DJ, Taga T, Khankaldyyan V, Schultz L, Fraser S, Nelson MD, Laug WE. Micro-MRI at 11.7 T of a murine brain tumor model using delayed contrast enhancement. Mol Imaging 2003;2:150–158.
5. Wright SM, McDougall M, Brown DG, Hazle J. Arrays of birdcage coils for imaging multiple samples. In: Proceedings of the ISMRM 9th Annual Meeting, Glasgow, 2001; p 18.
6. Matsuda Y, Utsuzawa S, Kurimoto T, Haishi T, Yamazaki Y, Kose K, Anno I, Marutani M. Super-parallel MR microscope. Magn Reson Med 2003;50:183–189.
7. Morris HD, Chesnik S. Two methods for multi-sample imaging: applications to mouse phenotyping via MRI. In: Proceeding of the ISMRM 9th Annual Meeting, Glasgow, 2001; p 19.
8. Xu S, Gade TP, Matei C, Zakian K, Alfieri AA, Hu X, Holland EC, Soghomonian S, Tjuvajev J, Ballon D, Koutcher JA. In vivo multiple-mouse imaging at 1.5 T. Magn Reson Med 2003;49:551–557.
9. Lazovic J, Stojkovic DS, Collins CM, Yang QX, Vaughan JT, Smith MB. Hexagonal zero mode TEM coil: a single-channel coil design for imaging multiple small animals. Magn Reson Med 2005;53:1150–1157.
10. Bock NA, Konyer NB, Henkelman RM. Multiple-mouse MRI. Magn Reson Med 2003;49:158–167.
11. Ohliger MA, Ledden P, McKenzie CA, Sodickson DK. Effects of inductive coupling on parallel MR image reconstructions. Magn Reson Med 2004;52:628–639.
12. Wong WH, Sukumar S. "Millipede" imaging coil design for high field micro imaging applications. In: Proceedings of the ISMRM 8th Annual Meeting, Denver, 2000; p 1399.
13. Kuo YT, Herlihy AH, So PW, Bhakoo KK, Bell JD. In vivo measurements of T1 relaxation times in mouse brain associated with different modes of systemic administration of manganese chloride. J Magn Reson Imaging 2005;21:334–339.
14. Watanabe T, Radulovic J, Spiess J, Natt O, Boretius S, Frahm J, Michaelis T. In vivo 3D MRI staining of the mouse hippocampal system using intracerebral injection of MnCl2. Neuroimage 2004;22:860–867.
15. Dazai J, Bock NA, Nieman BJ, Davidson LM, Henkelman RM, Chen XJ. Multiple mouse biological loading and monitoring system for MRI. Magn Reson Med 2004;52:709–715.
16. Nieman BJ, Chen XJ, Henkelman RM. Fast spin-echo sequence optimization for rapid T_2-weighted imaging at high field. In: Proceedings of the ISMRM 12th Annual Meeting, Kyoto, 2004; p 338.
17. Cassidy PJ, Schneider JE, Grieve SM, Lygate C, Neubauer S, Clarke K. Assessment of motion gating strategies for mouse magnetic resonance at high magnetic fields. J Magn Reson Imaging 2004;19:229–237.
18. Lenz GW, Haacke EM, White RD. Retrospective cardiac gating: a review of technical aspects and future directions. Magn Reson Imaging 1989;7:445–455.
19. Sutton BP, Ciobanu L, Zhang X, Webb A. Parallel imaging for NMR microscopy at 14.1 Tesla. Magn Reson Med 2005;54:9–13.